

# Femtosecond Laser Energy deposition in a M=3 Supersonic Flow: Parametric Study

*Paul-Quentin Elias\**

*\* DPHY, ONERA, Université Paris Saclay F-91123 Palaiseau -France*

*Nicolas Severac\*\*, Jean-Marc Luyssen\*\*, Jean-Pierre Tobeli\*\*, Reynald Bur\*\**

*\*\* DAAA, ONERA, Université Paris Saclay F-92190, Meudon – France*

*Ivan Doudet†, Benoît Wattellier†*

*† Phasics, Saint-Aubin ,F-91190, France*

*Yves-Bernard André‡, Sylvain Albert‡, André Mysyrowicz‡, Aurélien Houard‡*

*‡Laboratoire d'Optique Appliquée – ENSTA ParisTech - Ecole Polytechnique, Palaiseau, F-91761, France*

## Abstract

Femtosecond lasers can form long plasma filaments over distances ranging from several centimetres to several meters which can be used advantageously for high speed flow control, in particular for drag reduction. Recently the first experimental demonstration of femtosecond energy deposition in a wind tunnel has been reported. This paper completes this report by presenting a parametric analysis of the effect of the femtosecond energy deposition in the flow. In particular, the effect stagnation pressure on the flow perturbation and the drag variation is investigated. Drag measurements show that higher reductions in drag are obtained for larger stagnation pressures.

## 1. Introduction

Various non-standard control strategies are being considered for high-speed flow control, such as the use of surface of volume plasma actuators or laser energy deposition. This later technique is particularly appealing since it enables to control precisely the energy deposition location[1], [2]. However, most of the laser energy deposition techniques rely on nanosecond pulsed lasers which produce a localized plasma a few millimetres in size [3]. Using this plasma as a near continuous volume heat source requires a very high repetition rate which poses stringent requirements on the laser[4], [5]. Over the past few years, there have been some interests in using femtosecond lasers instead. Indeed, it has been suggested that the long filamentation[6], [7] that these class of lasers can produce can be used advantageously for high speed flow control [8], [9], in particular for drag reduction[10]. Contrary to nanosecond lasers, the plasma filament formed by the femtosecond laser pulses amounts to a nearly linear energy deposition with a length of up to ten centimetres and longer in certain instances[11]. Thus it is possible to maintain a nearly continuous energy deposition with a much lower repetition rate. Point *et al.* [12] have shown recently that significant gas heating can be obtained with femtosecond pulses only, provided that the pulse energy is large enough (energy range between 5 mJ and 250 mJ, pulse duration 50-200 fs). Temperature rise of several hundred Kelvin in air have been measured in a filamentary volume of length between 5 and 10 cm; in addition, the conversion efficiency of the pulse energy to heat can reach up to 60%. The linear energy deposition is in the range 0.1-4 mJ/cm, which is consistent with the requirements derived through parametric numerical simulations [10]. In addition, this avoids the use of a secondary power source. This key result has opened the way to an experimental demonstration of linear energy deposition in a supersonic flow.

Recently, the first experimental demonstration of the effect of femtosecond laser energy deposition has been carried out in ONERA R1Ch blow-down wind tunnel, showing in particular a dramatic effect of this linear energy deposition on the supersonic flow around a blunted test model[13]. The goal of this paper is to report on recent experiments aimed at demonstrating the « Laser Spike » concept. These experiments have been performed in Onera's R1Ch wind-tunnel, using the ENSTAMobile laser chain to produce ultrashort laser pulses in the TeraWatt range.

The first part of the paper will describe the experimental setup used for the experiments. The second part of the paper will present the results of this experimental investigations. First, the energy deposition in quiescent air will be described. Second, the effect of the femtosecond laser energy deposition in the M=3 airflow will be presented.

Schlieren characterization will show the details of the interaction and flow modifications. The drag and pressure measurements will also be presented and discussed. The effect of the stagnation pressure on the laser-flow interaction will also be discussed.

## **2.Experiment description**

### **2.1 Wind-tunnel**

The tests are performed in Onera's R1Ch blow-down wind tunnel. This facility is an open-jet wind-tunnel and uses a M=3 axisymmetric nozzle with an exit section 310 mm in diameter. The maximum stagnation conditions are 15 bar and 380 K for the pressure and temperature, respectively, yielding a maximum mass flow rate of 60 kg/s. When operating at low stagnation pressure (~3-5 bar) the test chamber is pumped down to facilitate the priming of the nozzle. The supersonic jet is collected and slowed down in a supersonic diffuser and collected in a 500 m<sup>3</sup> vacuum sphere.

For this project, the useful testing time varies between 15 s to 25 s, depending on the flow conditions. The range of stagnation pressure used in the experiments is:  $2.5 < P_i \text{ (bar)} < 8.5$ , for a stagnation temperature of ~305 K.

The terawatt laser is placed next to the wind-tunnel test section. The laser beam is guided using 3 inches mirror in the test chamber. After the focusing lens, the beam is guided inside the test model holding sting and emerges from a diaphragm at the tip of the model.

### **2.2 Test model**

The test model is a generic blunted body (HB2 shape[14]) which is a blunted cone (50° apex angle) with a base section of 60-mm in diameter (Figure 2). The nose of the model is hemispheric (radius 18 mm). As discussed above, the model is hollowed to provide an optical path for the laser beam. The tip of the model has a 3-mm diaphragm that provides the exit path for the focusing beam.

### **2.3 Laser system**

The EnstaMobile system is a research TW laser which can deliver laser pulses with a duration as low as 50 fs. Its centre wavelength is 800 nm and its maximum pulse energy measured at the tip of the test model is 150 mJ. The laser operates with a repetition frequency of 10 Hz. The laser master clock at 10 Hz defines the time reference for the synchronization of all the diagnostics used in the study. A fast photodiode is used to time the laser pulse.

The ultra-short laser pulse is focused with a lens and forms a plasma filament near the focal point of the lens [11], [15]. The location of the filament core in front of the model can be displaced by moving the focusing lens L

### **2.4 Drag balance**

The drag balance is composed of two parts:

- a weighted plate that holds the test model
- a fixed plate mounted on the holding sting

The resulting drag force acting on the weighted plate is measured using three piezoelectric Kistler force sensors (type 9134B) mounted at 120° around the model axis. These sensors measure the axial component of the drag. The overall sensitivity of the balance is 50 N/V.

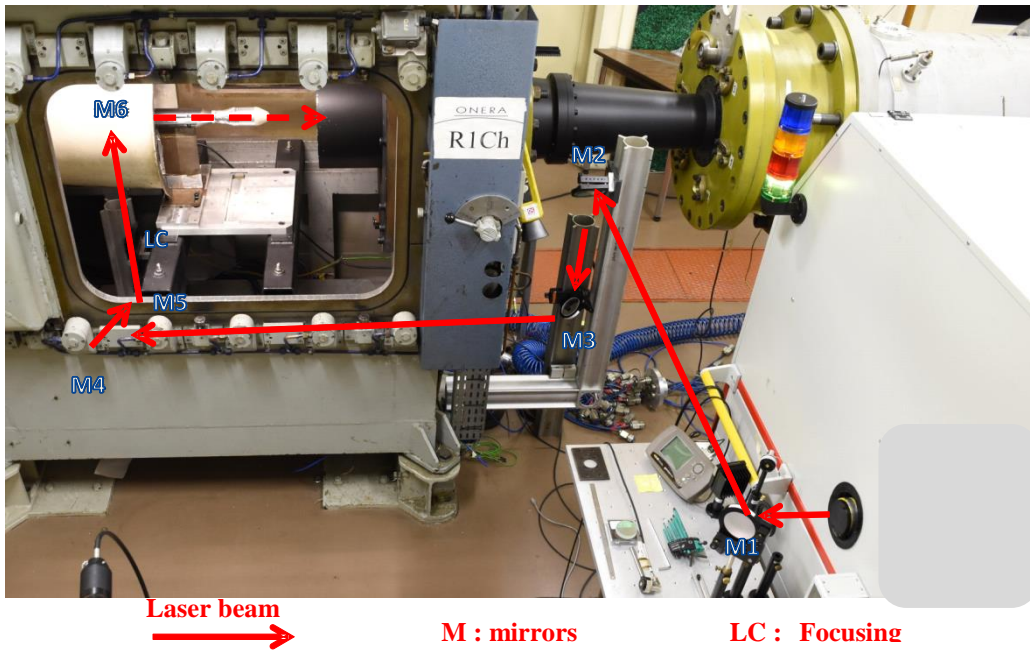


Figure 1 - Detail of the experimental setup. The top picture shows the R1Ch facility test section and the exit port of the Enstamobile laser. The laser beam path is shown in red. The detail of the injection in the test model is shown in the two detailed CAD views

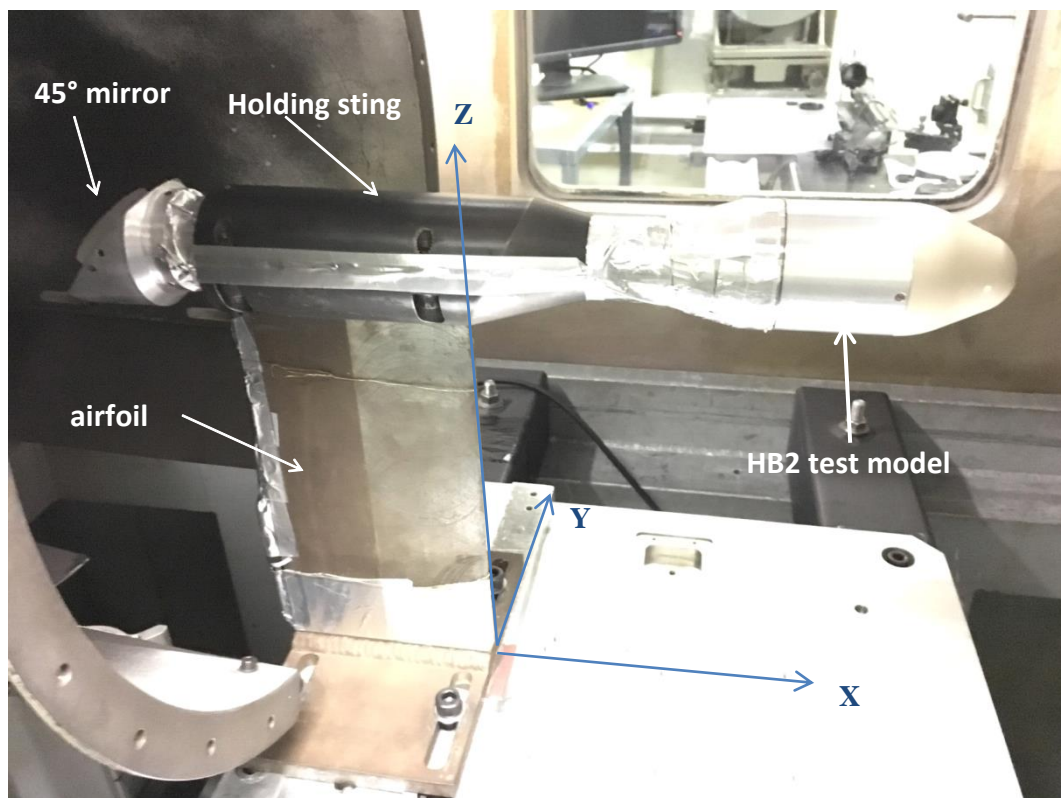


Figure 2 - View of the test model mounted in the R1Ch test section. The coordinate axes in the experiments are shown in blue. The model is located 160 mm downstream of the nozzle exit section.

## 2.5 Diagnostics

In addition to the internal drag balance, the model is fitted with two high-bandwidth pressures gauges (PCB 132A31). Their quoted bandwidth is 500 kHz.

The flow topology is characterized using a pulsed Schlieren system in a Z-configuration [16]. A pulsed laser diode (Cavitar Smart, central wavelength 688 nm) is used as the point light source (using an emission slit). A narrow bandpass optical filter centered on the laser wavelength is used on the detection side to filter out any stray light emitted by the ultra-short laser pulse, consisting mainly in a broadband emission. The nanosecond laser emits variable-length laser pulses. For this study, 100-ns long pulses are used. This duration is short enough to collect nearly instantaneous snapshots of the flow. The laser pulses are synchronized on the Enstamobile master clock, but with a controlled time delay. Owing the very good repeatability of the laser-flow interaction (see below), it is possible to probe different instants of the phenomena by gradually changing the delay.

### 3. Results

#### 3.1 Energy deposition in quiescent air

First, the effect of the laser pulses in quiescent air is investigated. This has already been investigated in a laboratory setup [12] using a Mach-Zender interferometer, in particular to measure the number density variations in the gas. Here, the goal is to check the location of the laser-induced quasi-linear energy deposition in front of the test model. The cumulated emission of several tens of laser pulses is shown in **Figure 3**.

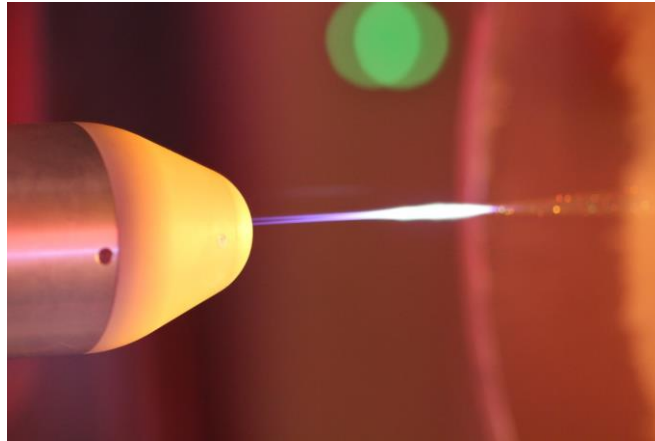
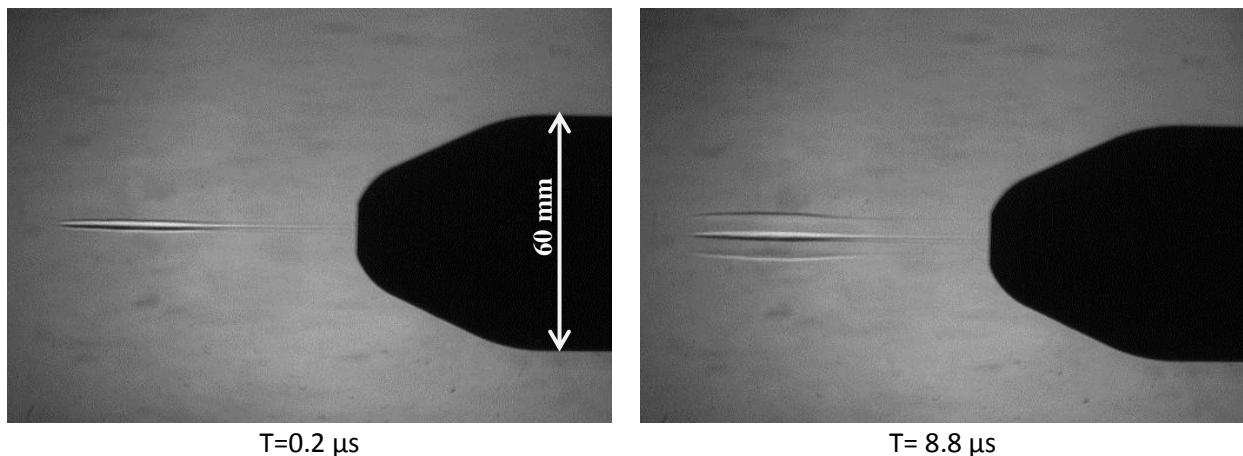


**Figure 3 – Long-exposure (4 s) image showing the cumulated emission of 40 laser pulses (50 fs, ~ 150 mJ/pulse) in quiescent air.**

The Schlieren images in Figure 4 show that the laser-induced plasma filament initially forms a central heated core (length ~60 mm). The plasma filament formed by the laser heats a column of gas. Compared to the characteristic timescale of the flow, this heating is nearly instantaneous. This causes a significant pressure rise in the heated core. The high-pressure relaxes in a quasi-cylindrical blast wave that expands radially ( $T = 8.8 \mu\text{s}$  and later). The heated channel relaxation is then driven by thermal conduction and natural convection, but with a much longer timescale (~ a few ms). The maximum diameter of the heated core is 5 mm, which is consistent with previous findings in a laboratory experiment [12].



$T=0.2 \mu\text{s}$

$T= 8.8 \mu\text{s}$

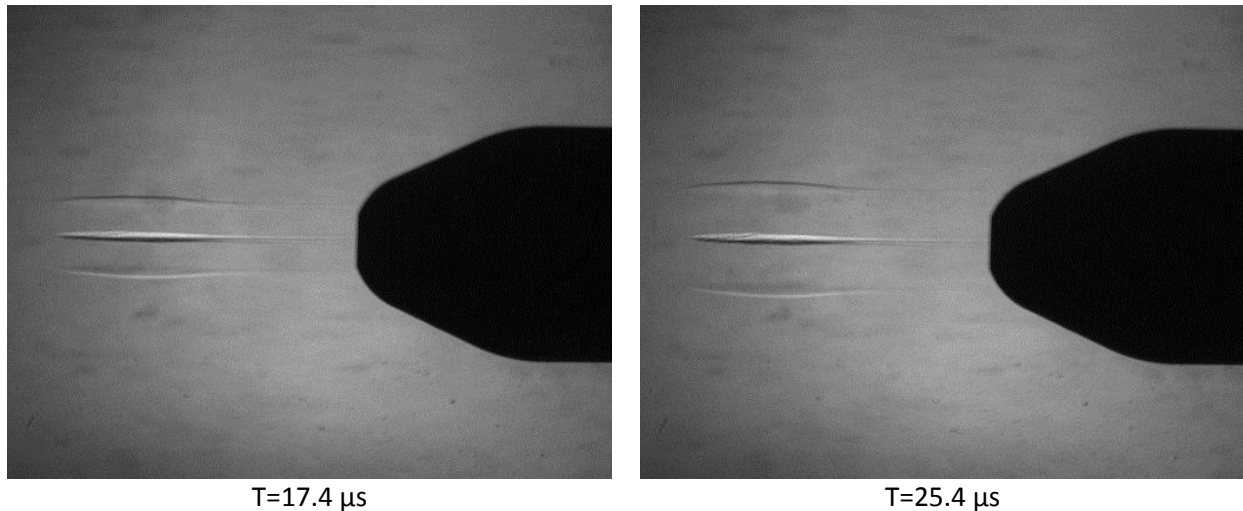


Figure 4 -Schlieren picture of the filamentary energy deposition upstream of the blunt body in quiescent air (ambient temperature, atmospheric pressure)

### 3.2 Energy deposition in a supersonic flow

When the test model is in the supersonic airflow, the activation of the ultra-short laser pulses induces a significant perturbation of the flow.

First, the drag balance signal shows that the laser-induced energy deposition cause significant fluctuations in the drag, as shown in Figure 5. The time evolution of the balance signal is typical of the results obtained for a variety of experimental conditions. First, one notices a slight increase of the drag, between 100  $\mu$ s and 170  $\mu$ s after the laser pulse. Then, the drag signal decreases sharply and then evolves roughly as a damped oscillator for 1-2 milliseconds. This behavior is entirely correlated to the laser activation, as shown in Figure 6.

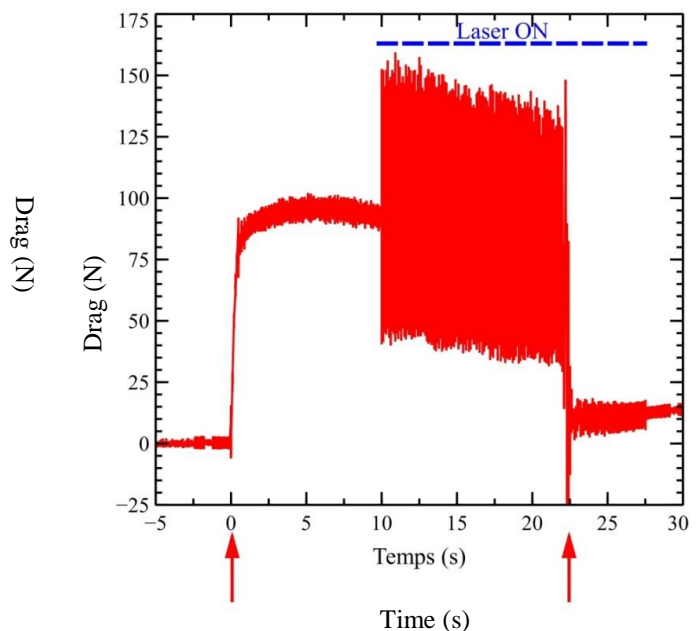
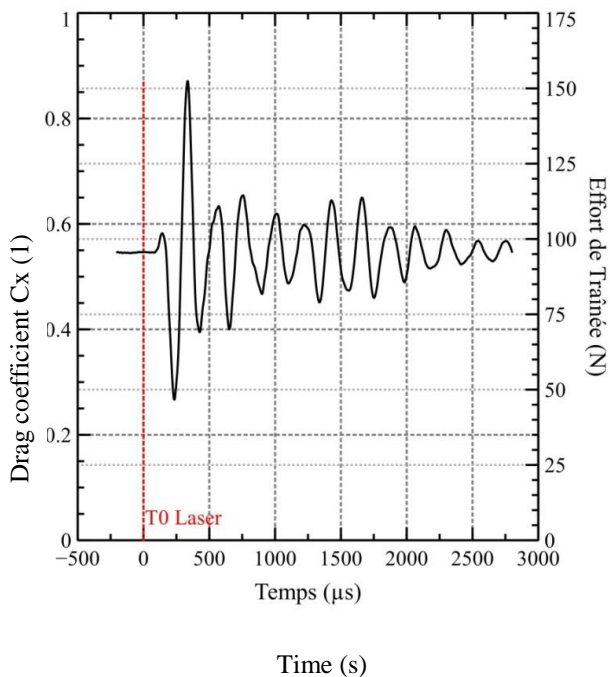


Figure 5 – Sample drag signal (test run 1632). The time axis is referenced to the laser pulse activation (dashed red line).

Figure 6 – Drag signal versus time (Test run 1628). The test starts at  $t=0$ . The laser is off for  $t=0$  to  $t=10$  s. It is turned on (operating at 10 Hz) at  $t=10$ s until  $t=27$  s. For each subsequent laser pulse, the drag signal exhibits an oscillating behavior.

The interaction of the heated channel created by the ultra-short laser pulse with the supersonic airflow is investigated for the test run 1632, typical of the results obtained in this study. The flow conditions for this run are given in Table 1. The laser operating conditions are given in Table 2.

Table 1 : Test run 1632 flow conditions.

Mach number	3,0
Stagnation Pressure (Pa)	$3,61 \times 10^5$
Stagnation Temperature (K)	309
Freestream pressure (Pa)	9 826
Freestream temperature (K)	110
Freestream gas density ( $\text{kg} \cdot \text{m}^{-3}$ )	0,31
Unit Reynolds number ( $\text{m}^{-1}$ )	$2,56 \times 10^7$
Freestream flow velocity ( $\text{m} \cdot \text{s}^{-1}$ )	631

Table 2 : Laser operation parameters, test run 1632.

Pulse energy ( laser output port) (mJ)	$170 \pm 10$
Focal length of focusing lens (mm)	1500
Approximate length of the energy deposition (mm)	$55 \pm 2$
Distance of the heated channel center to the nosetip (mm)	$25 \pm 2$

The laser pulse is generated every 100 ms (10 Hz repetition rate). During the whole test run, the signals from the drag balance and pressure sensors are recorded using a fast data acquisition system (2.5 Msamples / s). The Schlieren setup is used to recover the time evolution of the interaction. By changing progressively the time delay between the femtosecond pulse and the nanosecond laser pulse used to probe the flow, it is possible to recover the time evolution of the interaction with a good temporal resolution. This is possible because of the very good shot-to-shop repeatability of the phenomenon. The drag signal is very repeatable. The dispersion is greater for the unsteady pressure probes. This is caused by the turbulent pressure fluctuation during the interaction. The repeatability is further checked by set a fixed delay for the Schlieren laser pulse and checking that the flow features remains nearly unchanged.

Figure 7 and Figure 8 present the different phases of the interaction. First the formation of the heated channel and the cylindrical blast wave is observed ( $T_0+0.3 \mu\text{s}$  to  $T_0+8.9\mu\text{s}$ ), as in the tests in quiescent air (Figure 4). These features are also revealed in the zoomed viewed in **Erreur ! Source du renvoi introuvable.** The heated core is convected downstream and interacts with the detached bow shock. Because of the high temperature in the heated core, the flow becomes locally subsonic and enables the formation of a recirculating bubble expanding upstream from  $T_0+4.6 \mu\text{s}$  to  $T_0+35.7 \mu\text{s}$  in Figure 7 and **Erreur ! Source du renvoi introuvable.** Then the recirculating bubble expands radially between  $T_0+60.5 \mu\text{s}$  and  $T_0+112.1 \mu\text{s}$  (Figure 7 et Figure 8), and is convected downstream by the flow. One should note that, during this phase, the recirculating flow is probably turbulent. In addition, during the convection downstream of the bubble, the flow becomes unstable and no longer axisymmetric. The flow recovers its initial configuration approximately 250  $\mu\text{s}$  after the laser energy deposition.

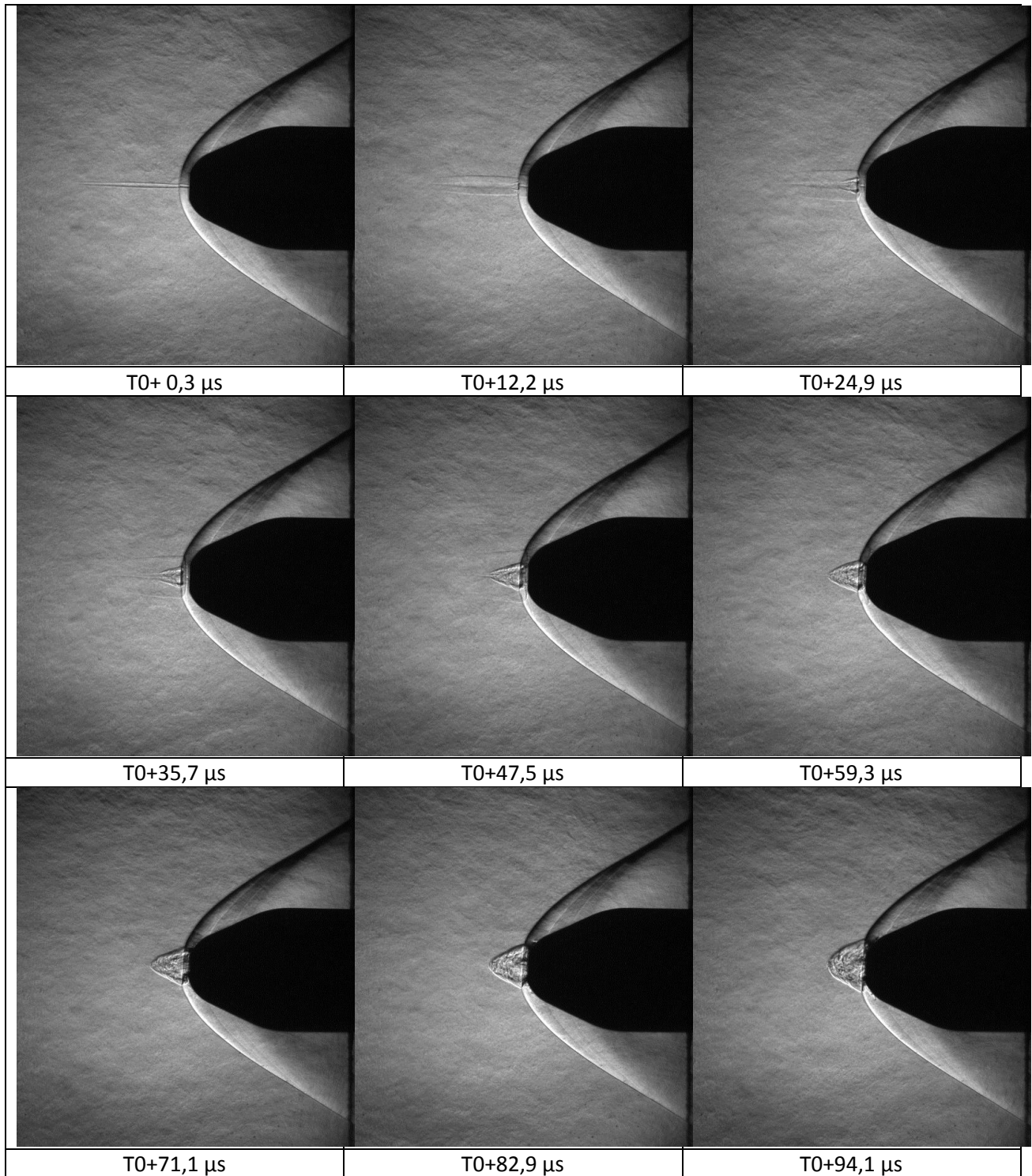


Figure 7 – Schlieren images of the flow during the interaction.

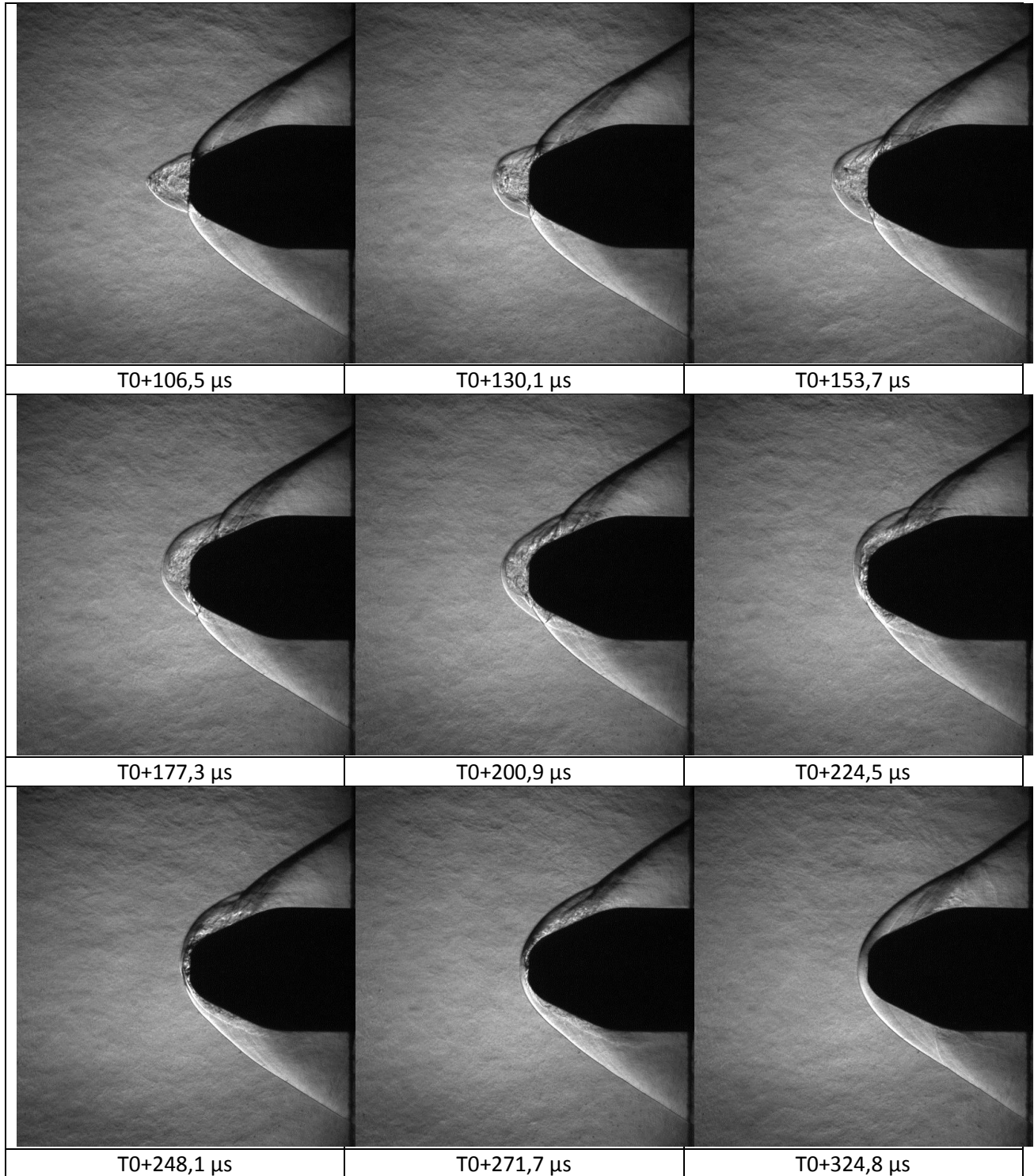


Figure 8- Schlieren images of the flow during the interaction.

### 3.3 Paramtric Study : Effect of the Stagnation pressure

The conditions used to study the effect of the stagnation pressure are shown in the Table.

Table 3 : Tests conditions for the stagnation pressure effect

Stagnation pressure (bar)	Freestream density (kg.m <sup>-3</sup> )	Unit Reynolds number (m <sup>-1</sup> )	Laser pulse energy (mJ)
2,5	0,184	$4,3 \times 10^6$	~ 150
3,5	0,257	$5,9 \times 10^6$	~ 150
5,5	0,404	$9,3 \times 10^6$	~ 150
7,5	0,551	$1,2 \times 10^7$	~ 150

Figure 9 shows the drag signals recorded for different stagnation pressures. The normalized curves can be used to compare the flow response during the interaction phase. We recall that the Schlieren images show that the flow recover its unperturbed state roughly 300 to 350  $\mu$ s after the laser energy deposition. This corresponds to the end of the first negative oscillation on the drag signal.

First, the normalized drag signals in Figure 9 show a slight increase of the drag 160 to 180  $\mu$ s after the deposition. The delay and intensity of this rise do not depend on the magnitude of the stagnation pressure. Second, the amplitude of pseudo oscillations of the drag increases the stagnation pressure increases.

The interaction of the energy deposition with the flow induces a nearly instantaneous reduction of the drag. Assuming that the balance behaves as a 2<sup>nd</sup> order system, it is possible to link the amplitude of the first negative oscillation to the mechanical impulse imparted on the test model. The analytical expression for a second order system gives the following expression for the oscillation amplitude:

$$s_{Min} = 2\pi f_0 K I_0 \quad (1)$$

Here,  $K = 0,02 V.N^{-1}$  is the static sensitivity factor of the balance,  $f_0$  is the pseudo-frequency of the first oscillation and  $I_0$  is the equivalent mechanical impulse, in N.s. This formula can be used with the measured drag signal to estimate the mechanical impulse. On each curve, the amplitude en pseudo period of the first negative oscillation is taken from the drag signal. These values are used to compute  $s_{Min}$  and  $f_0$  and from (1) on can compute the equivalent mechanical impulse.

The Figure 11 shows the mechanical impulse as the function of the stagnation pressure . The larger the stagnation pressure, the larger the mechanical impulse is, meaning the drag reduction magnitude increases. This increase is not. When the stagnation pressure triples (from 2,5 bar to 7,5 bar), the mechanical impulse doubles. This suggests that there is a saturation phenomenon in the interaction. Additionally, on can link this increase to the larger fraction of energy deposited in the flow by the plasma filament when the gas density increases. Indeed, the upstream gas density is 0,18 kg.m<sup>-3</sup> for 2,5 bar of stagnation pressure, which is one sixth of the atmospheric gas density. Energy deposition tests in static conditions have shown the higher the gas density, the high the fraction of energy deposited is.

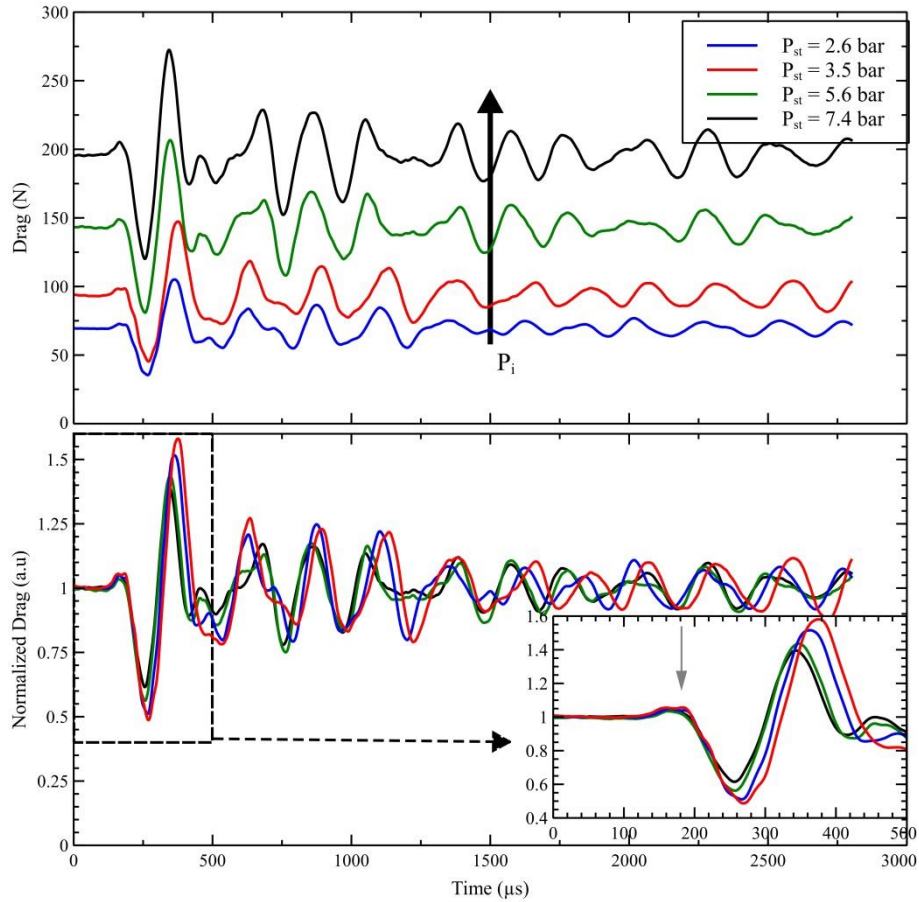
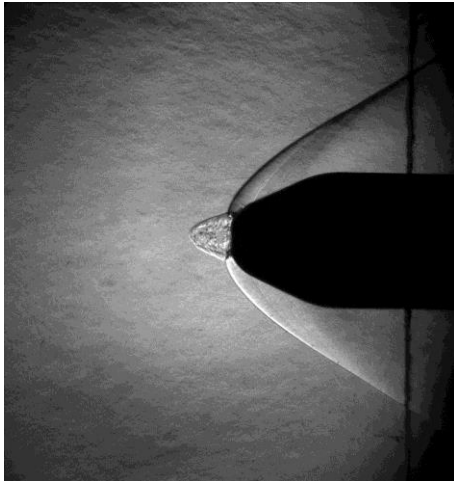
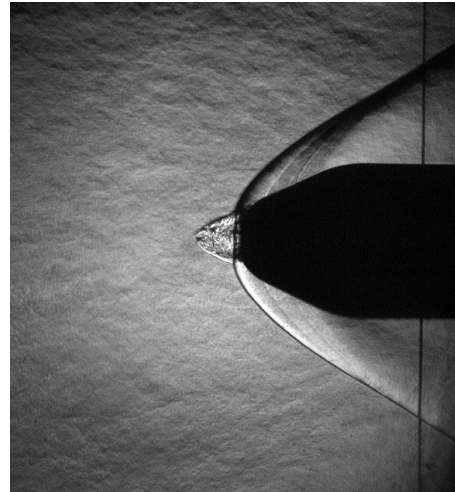


Figure 9 – Drag signal vs time (top frame) for different stagnation pressure. The bottom graphs show the normalized signals. The time  $t=0$  is the laser energy pulse instant.



$T_0+107 \mu s$ ,  $P_{st}=2,5 \text{ bar}$ . Recirculating bubble size : 19 mm



$T_0+109 \mu s$ ,  $P_{st}=7,5 \text{ bar}$ . Recirculating bubble size : 19 mm

Figure 10 – Schlieren images showing the recirculating bubble formed 100  $\mu s$  after the laser energy deposition.

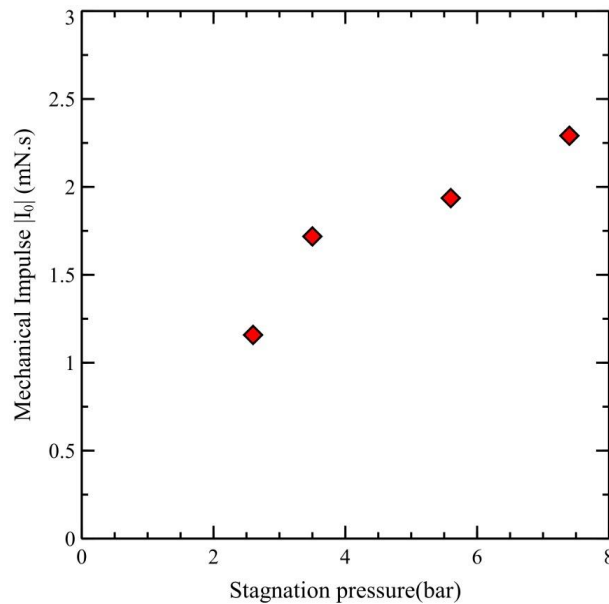


Figure 11 – Mechanical impulse as a function of the stagnation pressure.

#### 4. Conclusion

In this study, the significant effect of femtosecond filaments on a supersonic flow has been experimentally demonstrated. It has been found that the low-energy laser spike ( $\sim 10$  mJ deposited) induces a significant transient reduction of the drag. The plasma filament created by the ultra-short laser pulse forms a low-density heated core that interacts with the detach bow shock. This interaction produces an inflating recirculating bubble and leads to a transient reduction of the drag. This effect increases non-linearly with the stagnation pressure, meaning that higher energy deposition efficiency is reached when the upstream density (stagnation pressure) increases. The observations reported here demonstrate the potential interest of ultra-short laser for flow control applications. Further work will have to address the effect of repetitive laser pulses to obtain a quasi-steady effect on the flow.

#### 5. References

- [1] H. Yan, R. Adelgren, and M. Boguszko, "Laser energy deposition in quiescent air," *AIAA J.*, vol. 41, no. 10, pp. 1988–1995, 2003.
- [2] H. Yan, "Control of Edney IV Interaction by Energy Pulse," *AIAA J.*, vol. 43, no. January, pp. 9–12, 2006.
- [3] N. G. Glumac, G. S. Elliott, and M. Boguszko, "Temporal and Spatial Evolution of a Laser Spark in Air," *AIAA J.*, vol. 43, no. 9, pp. 1984–1994, 2005.
- [4] A. Iwakawa, N. Hasegawa, T. Osuka, R. Majima, T. Sakai, and A. Sasoh, "Supersonic Drag Reduction Performance of Blunt-Body with Conical Spike using Energy Depositions," in *44th AIAA Plasmadynamics and Lasers Conference*, 2013.
- [5] J.-H. Kim, A. Matsuda, T. Sakai, and A. Sasoh, "Wave Drag Reduction with Acting Spike Induced by Laser-Pulse Energy Depositions," *AIAA J.*, vol. 49, no. 9, pp. 2076–2078, Sep. 2011.
- [6] A. Houard, Y. Liu, and A. Mysyrowicz, "Recent developments in femtosecond filamentation," *J. Phys. Conf. Ser.*, vol. 497, p. 012001, Apr. 2014.
- [7] A. Couairon and A. Mysyrowicz, "Femtosecond filamentation in transparent media," *Phys. Rep.*, vol. 441, no. 2–4, pp. 47–189, 2007.
- [8] K. Kremeyer, K. Sebastian, and C. Shu, "Lines of pulsed energy : shock mitigation and drag reduction," in *42nd AIAA Aerospace Sciences Meeting and Exhibit*, 2004.
- [9] V. R. Soloviev *et al.*, "Drag Reduction by Plasma Filaments over Supersonic Forebodies," *AIAA J.*, vol. 41, no. 12, pp. 2403–2409, Dec. 2003.
- [10] P. Elias, "Numerical Simulations on the Effect and Efficiency of Long Linear Energy Deposition Ahead of a Supersonic Blunt Body : Toward a Laser Spike," *Aerosp. Lab J.*, no. 10, pp. 1–11, 2015.

- [11] M. Durand *et al.*, “Kilometer range filamentation,” *Opt. Express*, vol. 21, no. 22, p. 26836, Nov. 2013.
- [12] G. Point, E. Thouin, A. Mysyrowicz, and A. Houard, “Energy deposition from focused terawatt laser pulses in air undergoing multifilamentation,” *Opt. Express*, vol. 24, no. 6, p. 6271, 2016.
- [13] P. Q. Elias *et al.*, “Improving supersonic flights with femtosecond laser filamentation,” *Sci. Adv.*, vol. 4, no. 11, 2018.
- [14] R. Cérésuela, “Mesure d’efforts et de pression sur la maquette balistique étalon HB2,” 1964.
- [15] A. Couairon and A. Mysyrowicz, “Femtosecond filamentation in air,” *Prog. Ultrafast Intense Laser Sci.*, vol. 84, pp. 235–258, 2006.
- [16] G. S. Settles, *Schlieren and Shadowgraph Techniques: Visualizing Phenomena in Transparent Media*. Springer, 2001.